Probing the unfolded protein response to mouse hepatitis coronavirus infection through RNA sequencing and ribosome profiling

Georgia M. Cook[1], Katherine Brown[1], Krzysztof Franaszek[1], Nathan A. Moore[2,4], Stuart G. Siddell[2], Ian Brierley[1], Andrew E. Firth[1], Nerea Irigoyen[1]*

[1]Division of Virology, Department of Pathology, University of Cambridge, Tennis Court Road, Cambridge CB2 1QP, United Kingdom.

[2]Department of Cellular and Molecular Medicine, University of Bristol, Bristol BS8 1TD, United Kingdom.

[4]Current address: Basingstoke and North Hampshire Hospital, Hampshire Hospitals, NHS Foundation Trust.

Running Title: Unfolded protein response to coronavirus infection

*Corresponding author: ni236@cam.ac.uk

Keywords: murine coronavirus, ribosome profiling, RNASeq, unfolded protein response, translation, protein synthesis.

Abstract:

Coronaviruses (CoVs) are enveloped, positive-sense RNA viruses with an unusually large RNA genome and a unique replication strategy. They cause important diseases in mammals and birds ranging from enteritis in cows and pigs and upper respiratory disease in chickens, to potentially lethal human respiratory infections. Here, we apply ribosome profiling and parallel RNA sequencing to analyse global changes in host cell transcriptome and translatome upon infection with mouse hepatitis virus strain A59 (MHV-A59), a model murine coronavirus in the same genus as the human pathogens severe acute respiratory syndrome coronavirus (SARS-CoV) and Middle East respiratory syndrome coronavirus (MERS-CoV). Amongst differentially-regulated cellular genes, we observed up-regulation of all arms of the unfolded protein response (UPR), including translational activation of transcription factors ATF4, ATF5 and Chop. Polysome profiling of infected-cells revealed an accumulation of empty 80S ribosomes, consistent with increased phosphorylation of eIF2α leading to translational shut-off via inhibited initiation. Ribosomal footprints on phosphorylated-eIF2α-resistant mRNAs revealed unambiguous upstream open reading frame (uORF) occupancy consistent with host maintenance of the UPR. Unexpectedly, an inhibitor of PERK that blocks the UPR and relieves translation inhibition was found to attenuate virus growth suggesting that MHV may subvert the UPR to its own advantage. This study sheds new light on the complex interactions between MHV and host during infection and provides new potential targets for antiviral intervention.

Introduction

The *Coronaviridae* are a family of enveloped viruses with positive-sense, monopartite, single-stranded RNA genomes. At 27–32 kb, coronaviruses (CoVs) have the largest known RNA genomes. CoVs cause a broad range of diseases in animals and humans, ranging from the common cold to severe acute respiratory syndrome (SARS) [1]. Amongst CoVs of medical importance with high mortality rates and pandemic potential are SARS-CoV and MERS-CoV, both members of the

genus *Betacoronavirus.* Murine coronavirus, a betacoronavirus more commonly refered to as mouse hepatitis virus (MHV), has been used as a model to study the replication and biology of members of this genus.

Virus infection alters cellular gene expression to facilitate replication of the viral genome and the assembly of virus particles. As with all viruses, CoVs rely on the host cell translational machinery for viral protein synthesis. Many viruses have evolved mechanisms to shut off host mRNA translation, which can increase the availability of the translational machinery for non-canonical modes of viral protein synthesis, and at the same time inhibit host antiviral responses [2]. Exactly how CoVs induce host translational shut-off and its significance in relation to the synthesis of virus proteins, particularly at later times of infection, is still poorly understood. During CoV replication, the massive production and modification of viral proteins, as well as virion budding-related endoplasmic reticulum (ER) membrane depletion, can lead to overloading of the folding capacity of the ER and, consequently, ER stress [3]. This activates the unfolded protein response (UPR) which returns the cell to homeostasis and mitigates the major risks that protein misfolding poses for correct cellular function [4]. In mammalian cells, the UPR is controlled by three ER-resident transmembrane sensors: the inositol-requiring enzyme-1 (IRE1), the PKR-like ER kinase (PERK), and the activating transcription factor-6 (ATF6). These sensors recognise unfolded/misfolded proteins inside the ER and transmit a signal to the nucleus to transcribe specific genes whose products act to decrease protein synthesis and increase ER folding capacity [4]. Previous studies (reviewed in [5]) have aimed to establish how the different UPR pathways are involved during CoV infection.

Ribosome profiling (RiboSeq) allows global monitoring of cellular translation by mapping the positions of translating ribosomes on the transcriptome [6-8]. RiboSeq reveals the location and abundance of ribosomes on specific mRNA species with single-nucleotide precision. In conjunction

with RNASeq, to determine the corresponding transcriptome, RiboSeq has been used to elucidate changes in translation, transcription and translation efficiency in viral and host gene expression during the course of infection [9-19].

Here, we use RiboSeq and parallel RNASeq to analyse global changes in the host translatome and transcriptome throughout a time course of CoV infection. We observe activation of different pathways of the UPR leading to eIF2α phosphorylation and translational shut-off at the level of initiation which we confirm by polysome profiling. Surprisingly, a pharmacological inhibitor of the UPR was found to mildly attenuate virus replication, suggesting that MHV may subvert the UPR to its own advantage. This detailed analysis of cellular translation during MHV infection provides new insights into the mechanism of CoV translational shut-off and the complex interactions between virus and host during infection, and may aid the identification of new targets for antiviral intervention.

Results:

Effects of MHV-A59 infection on cellular gene expression

To survey genome-wide changes in host translation and transcription during CoV-infection, murine 17 clone 1 cells (17Cl-1) were infected with recombinant MHV-A59 at a multiplicity of infection (MOI) of 10. Two independent biological replicates of infected and mock-infected cells were harvested at 5 hours post-infection (h p.i.) and one replicate at 8 h p.i. Lysates were subjected to ribosome profiling and parallel RNASeq. In ribosome profiling, infected cell lysates are treated with RNase I and 28-32 nt long ribosome-protected fragments (RPFs) purified and processed for high-throughput sequencing. The resultant reads are mapped onto viral and host genomes, allowing the positions of translating ribosomes to be determined at sub-codon resolution. We found that a commonly-included additional step, in which cells are incubated with cycloheximide (CHX) before

lysis, caused stress-induced accumulation of ribosomes at the 5´ end of coding regions (CDSs; [16]). In this work, therefore, cells were not pretreated with CHX and were snap-frozen before lysis, which avoids this artefact (Supplementary Figure 1, [20]).

Effects of MHV-A59 infection on cellular transcription

To assess the effects of MHV infection on cellular transcript abundance at 5 h p.i., differential expression analysis was performed on two biological replicates with DESeq2 [21]. Between infected and mock-infected conditions, genes with a fold change ≥2 and a false discovery rate (FDR)-corrected *p* value of ≤0.05 were considered to be significantly differentially transcribed (Fig 1A, Supplementary Table 1). Some of the most differentially transcribed cellular genes (ochre points) are related to the host translational apparatus: *Rplp1* – a ribosomal protein from the large subunit; *Eef1a1* – eukaryotic elongation factor 1A-1; *Rps21* – a ribosomal protein from the small subunit; *Eif3f* – eukaryotic initiation factor 3 subunit F; *Eif3j1* – eukaryotic initiation factor 3 subunit J; and *Eif2b3*. This is also reflected in the gene ontology (GO) term enrichment analysis (Fig 1B; full results in Supplementary Table 2), which reveals that all GO terms enriched in the list of genes significantly transcriptionally down-regulated in infection were related to protein synthesis (blue points).

Several transcription-related genes were found to be transcriptionally up-regulated, for example *Polr2a*, the gene coding for the largest subunit of RNA polymerase II (Fig 1A). GO terms related to transcription, for example “transcription by RNAPII” (GO:0006366), are also enriched in the up-regulated genes list. Many histones feature in the transcriptionally up-regulated gene list and, as such, many histone-related GO terms are enriched in this list (Fig. 1B). Significantly, the GO term “response to unfolded protein” (GO:0006986) is enriched 4.85-fold in the list of genes transcriptionally up-regulated during infection (p=0.046, FDR-adjusted p-value), with similar fold

changes observed for "response to topologically incorrect protein" (GO:0035966; 4.31-fold enrichment; p=0.046) (Supplementary Table 2) and "response to endoplasmic reticulum stress" (GO:0034976; 3.8-fold enrichment; p=0.012) (Fig 1B – note that these terms are clustered within the "response to unfolded protein" GO term). Accordingly, some of the most differentially expressed genes were involved in the UPR such as *Herpud1* – homocysteine inducible ER protein with ubiquitin like domain 1; *Bip* - immunoglobulin heavy chain-binding protein; *Chac1* – glutathione-specific gamma-glutamylcyclotransferase 1; *Chop* - a C/EBP family transcription factor involved in the ER stress response, and *Xbp1* - X-Box Binding Protein 1 (Fig 1A). As the replication cycle of CoVs is known to be intimately linked to the ER, and previous studies have used different techniques to infer information about how CoV infection affects different branches of the UPR, we decided to focus on this area.

To validate changes in the transcript abundance of these genes, total RNA was extracted from three biological replicates of MHV-infected and mock-infected cells at 5 h p.i. and the levels of selected up-regulated (Fig 1C, left panel) and down-regulated (Fig 1C, right panel) transcripts assessed by quantitative real-time PCR (qRT-PCR), normalised by a 'housekeeping gene', ribosomal protein L19 (*Rpl19*), which has been reported to be unaffected by ER stress [22,23]. Up-regulated transcripts had qRT-PCR values broadly consistent with the RNASeq measurements (Fig 1A and 1C) whereas there was a little more variation in the down-regulated transcripts, which may be partly explained by the observation that *Rpl19* itself was slightly, though not statistically significantly, down-regulated ($\log_2$(fold change) = -0.34, p=0.37) (Fig 1A, yellow).

Effects of MHV-A59 infection on cellular translation

CoVs induce host translational shut-off [24-29] although the mechanisms are not completely understood. We reasoned that some host genes may be resistant to virus-induced shut-off and that identifying such genes might give new insights into the shut-off mechanism(s). To evaluate

differences at the level of translation as a result of MHV infection, we calculated relative translation efficiencies (TE) – defined herein as the ratio of ribosome-protected-fragment (RPF) and total RNA density in the CDS of a given gene – at 5 h p.i. using Xtail [30], applying the same fold change and *p*-value thresholds as for the transcription analysis. As shown in Fig 2A, several of the translationally up-regulated genes encode key proteins involved in activation of the UPR, for example ATF4 (activating transcription factor 4), ATF5 (activating transcription factor 5) and CHOP (DDIT3/GADD153) which are effector transcription factors [31-36]. GADD34 (MYD116/PPP1R15A), a protein that acts as a negative regulator to diminish UPR activation if persistent for a long time [37,38], is also translationally up-regulated.

Phosphorylation of eukaryotic initiation factor (eIF) 2α is a well-known mechanism for translational shut-off, and can also result from UPR activation, so we next investigated whether the mRNAs found to be preferentially translated during MHV infection were enriched for genes resistant to translational repression by phosphorylated eIF2α (p-eIF2α). This is not an existing GO term but, using a pre-existing list of p-eIF2α resistant genes published in Andreev *et al* [36] (Supplementary Table 2), an enrichment analysis compared to a background of all expressed genes demonstrated a 9.15-fold enrichment of mRNAs annotated with this term with a *p*-value of 1.42×10^{-4} (Fisher Exact Test).

Resistance to the effects of p-eIF2α has been linked to the presence of efficiently translated upstream open reading frames (uORFs) in the 5´ UTR of these mRNAs, which allow ribosomes to undergo selective re-initiation of the main ORF under conditions of eIF2α phosphorylation [31-36,39]. Our RiboSeq data were of sufficiently high resolution to determine reading frame and thus unambiguously assign ribosome occupancy to several uORFs on eIF2α-resistant mRNAs (for example *Atf5*, *Gadd34*, *Slc35a4* in Supplementary Fig 2). Comparison of RPF distribution with RNASeq read distribution allows visualisation of the changes in TE. These results, consistent with

eIF2α phosphorylation (leading to inhibited translation initiation), could indicate a major cause of host translational shut-off during MHV infection. This will be further explored below.

Comparison of transcriptional and translational changes during MHV-A59 infection

A comparison of the effects of MHV infection on both transcription and translation of individual cellular mRNAs is shown in Figure 2 (panel B). In some cases, for example *Polr2a*, the up-regulation of transcription is accompanied by down-regulation of TE (or vice versa); this leads to a buffering effect that presumably results in relatively minor changes in protein levels. The top-centre section of Fig. 2B shows genes that are transcriptionally up-regulated without any significant change in TE (blue dots). Consistent with this, *Chac1*, *Herpud1*, *Bip* and *Xbp1* are induced transcriptionally by factors involved in UPR activation, but do not have increased TE as they are not resistant to eIF2α phosphorylation [40-43]. *Atf4*, *Slc35a4* and *Atf5*, in the lower right hand quadrant of Fig 2B, are translationally resistant to p-eIF2α but not transcriptionally induced by the activation of UPR [32-36]. *Gadd34* and *Chop*, in the upper right hand quadrant of Fig 2B, are both translationally resistant to p-eIF2α and transcriptionally induced by ATF4 [35,39,44-45]. However, this transcriptional up-regulation is only statistically significant for *Chop*, setting it apart as a rare example of a gene that is both transcriptionally and translationally up-regulated in MHV infection.

MHV infection and activation of the unfolded protein response

Although several studies [27, 46-48] have aimed to establish how each of the three UPR sensor pathways may be involved during CoV infection, we wanted to take advantage of the data that ribosome profiling provides to carry out a comprehensive analysis of specific arm of the UPR response during MHV infection. In the mouse gene ontology database, the GO categories for each of the three specific branches of the UPR activation, are too small for meaningful inclusion in the enrichment analysis, probably due to incomplete annotation of these pathways in *Mus musculus*. In order to analyse enrichment of UPR-related functions more thoroughly, lists of significantly

differentially expressed genes were mapped to human orthologues and used for Reactome pathway enrichment analysis [49]. In this analysis, UPR (R-HSA-381119) was the most significantly enriched pathway attributed to transcriptionally up-regulated genes, with the ATF6 branch (R-HSA-381183) second, and the other two branches (PERK-ATF4 and IRE1α: R-HSA-380994 and R-HSA-381070) further down the list (Supplementary Table 3).

Monitoring IRE1α and ATF6

ER stress induction activates endonuclease IRE1α which cleaves X-box binding protein-1 (*Xbp-1*) mRNA [43,50]. Activated IRE1α removes a 26-nt intron from unspliced *Xbp-1* (*Xbp-1u*) mRNA leading to a translational reading frame shift and a longer protein. The product of spliced *Xbp-1* mRNA (*XBP-1s*) is an active transcription factor that up-regulates the expression of ER-associated degradation (ERAD) components and ER chaperones. 17 Cl-1 cells were infected with MHV-A59 or incubated with tunicamycin, a pharmacological inducer of ER stress which activates all UPR signalling pathways. Determination of *Xbp-1* splicing was done by reverse transcriptase PCR (RT-PCR) of total RNA extracted from 17 Cl-1 cells infected with MHV-A59 at 2.5, 5, 8 and 10 h p.i. or incubated with tunicamycin, using specific primers flanking the *Xbp-1* splice site (Fig 3A). At all timepoints, *Xbp-1u* was the predominant form in mock-infected cells whereas *Xbp-1s* was the major species in tunicamycin-treated cells. In virus-infected cells, *Xbp-1u* was predominant at 2.5 h p.i. but *Xbp-1s* became predominant at 5 h p.i.. An apparent reduction of RNA levels of *Xbp-1* and *Rpl19* can be seen at 8 and 10 h p.i. but this is likely due to the fact that RT reactions were carried out using a consistent amount of total RNA as starting material but, at these timepoints, viral RNA comprises approximately 80% of the total RNA in the cell [16]. In order to analyse translation of *Xbp-1u* and *Xbp-1s* in virus-infected cells, we inspected the ribosome profiling data (Fig 3B). For MHV-infected cells (MHV RiboSeq panels) and tunicamycin-treated cells (RiboSeq Tunicamycin panel), an increased number of reads mapped in the +2 reading frame (yellow peaks) corresponding to the *Xbp-1u* sequence, and downstream of the annotated main ORF stop codon (pink dashed line).

These reads result from translation of the *Xbp-1s* frameshifted isoform and indicate a dramatic increase in production of the active transcription factor.

Upon induction of ER stress, ATF6 translocates from the ER to the Golgi apparatus where it is cleaved by the proteases Site-1 (S1P) and Site-2 (S2P) [51]. After cleavage, the amino-terminus of ATF6, containing a basic leucine zipper (bZIP) transactivating domain, translocates to the nucleus to up-regulate the ER chaperone immunoglobulin heavy chain binding protein (BiP). 17 Cl-1 cells were infected with MHV-A59 or incubated with tunicamycin and analysed by Western blot for ATF6 cleavage upon ER stress induction (Supplementary Figure 3A upper panel). However, we were unable to detect any differences in the blots of mock-infected, MHV-infected or tunicamycin-treated cells. Therefore, to analyse this UPR branch, we monitored BiP, whose mRNA or protein levels serve as a proxy for activation of the ATF6 pathway (although its transcription can eventually be regulated by other UPR factors such as XBP-1 and CHOP) [27,52]. Cells were harvested at 2.5, 5, 8 and 10 h p.i. and analysed by qRT-PCR in three biological replicates (plotted as the ratio of transcription of *BiP* to the house-keeping gene *Rpl19*: Fig 3C). An increase in *BiP* transcription compared to the house-keeping gene *Rpl19* was observed in tunicamycin-treated (purple) and MHV-infected cells (orange) from 2.5 to 8 h p.i. followed by a modest decline, whereas mock-infected cells (blue) showed no induction. Surprisingly, whereas Western blot analysis (Fig 3D) confirmed induction of BiP protein in tunicamycin-treated cells by 8 h p.i., no such induction was seen in MHV-infected cells. RNASeq and RiboSeq read counts of *BiP* at 5 and 8 h p.i. (Fig 2B and Supp Fig 3B), revealed an increase in RNASeq reads in MHV-infected cells (Supplementary Figure 3B; Mock RNASeq compared to MHV RNASeq panels) consistent with the qRT-PCR results. Although an expected increase in RPFs was seen in infection (Supplementary Figure 3B; MHV RiboSeq panels), ribosome density was quite low in comparison to tunicamycin treated cells (6 h) (Supplementary Figure 3B; RiboSeq Tunicamycin panel) and perhaps beyond the detection limit of the immunoblots of Fig. 3D.

Monitoring PERK-eIF2α -ATF4 activity

In response to ER stress, PERK oligomerises and auto-phosphorylates [53]. Activated PERK phosphorylates the α-subunit of eukaryotic initiation factor 2 (eIF2α) which in turn impairs recycling of inactive eIF2-GDP to active eIF2-GTP resulting in a general shutdown of protein synthesis [54]. However, as previously described, translation of ATF4 is increased in this situation [31,32,55] leading to the induction of its target gene *Chop*. To monitor activation of this pathway, we analysed PERK, CHOP, ATF4 and p-eIF2α expression by qRT-PCR and Western blotting. 17 Cl-1 cells were infected with MHV-A59 or incubated with tunicamycin for 2.5, 5, 8 and 10 h. As shown in Fig 4A, *Chop* mRNA levels (measured as the *Chop/RpL19* ratio) increased five-fold in tunicamycin-treated cells (purple) compared to mock-infected cells (blue), and were stable over the time course. In MHV-infected cells (orange), the ratio also increased from 2.5 to 8 h p.i. although not to the level seen in tunicamycin-treated cells. Protein expression was determined by immunoblotting using antibodies specific for MHV nucleocapsid protein (N), PERK, ATF4, p-eIF2α and eIF2α, with GAPDH and eIF2α as loading controls (Fig 4B). PERK, ATF4, p-eIF2α and eIF2α □ere at all time points in both tunicamycin-treated and MHV-infected cells (from 5 h p.i. onwards). The multiple bands observed for PERK correspond to autophosphorylated species, indicative of the activation of this kinase upon ER stress. To rule out the possibility that eIF2α might also be phosphorylated as a response to protein kinase R (PKR) activation, we confirmed the absence of phosphorylated PKR in Western blots (Supplementary Figure 3A, lower panel).

Subsequently, we analysed profiles of RiboSeq and RNASeq reads mapping to ATF4 in virus-infected and tunicamycin-treated cells (Fig 4C). Consistent with previous studies [31,32], translation of the short (three codon) uORF1 (frame +2, yellow reads, nucleotides 399 to 407) was observed under all conditions. In mock-infected cells, uORF2 was efficiently translated (Mock RiboSeq panels; reads in yellow mapping to uORF2 indicated by a yellow rectangle, frame +2) thus diverting scanning preinitiation ribosomes from accessing the main ORF (pink rectangle) to which

very few RPFs mapped. In contrast, in MHV-infected cells (MHV RiboSeq panels), a substantial fraction of preinitation ribosomes were able to scan past uORF2 to translate the main ORF, leading to a reduced density of ribosomes on uORF2 and a greatly increased number of RPFs mapping to the main ORF. Tunicamycin-treated cells showed an intermediate ribosome distribution, but again with efficient translation of the main ORF.

Polysome profiling of 17 Cl-1 cells infected with MHV-A59

Since total read counts are normalised by library size, ribosome profiling does not provide information on total global translation levels. To further investigate virus-induced inhibition of translation as a consequence of UPR activation and eIF2α phosphorylation, analytical polysome profiling (Fig 5A) was performed for mock- and MHV-infected 17 Cl-1 cells. Cytoplasmic extracts were prepared in the presence of cycloheximide to retain intact monosomes and polysomes and analysed by sucrose density gradient centrifugation. This revealed an accumulation of monosomes (80S) in MHV-infected cells from 5 h p.i. onwards, consistent with inhibition of initiation. To investigate whether the 80S ribosomes accumulating during MHV infection contain mRNA (as an indicator of a translating ribosome), polysome profiling was repeated using a higher salt buffer (400 mM KCl; Fig 5B): a condition in which 80S ribosomes lacking mRNA dissociate into constituent subunits. In mock-infected cells, a modest diminution of 80S levels was observed at 400 mM KCl (mock 5 h, compare Fig 5A panel 2, and Fig 5B left panel), but a much greater reduction in 80S was observed in MHV-infected cells (MHV 5 h p.i., compare Fig 5A panel 5 and Fig 5B right panel), indicating that the vast majority of 80S ribosomes accumulating at this time point are not mRNA-associated. These data support the view that MHV-infection leads to translational shut-off via inhibited initiation, consistent with the effects of eIF2α phosphorylation.

Effect of the PERK inhibitor GSK-2606414 on MHV replication

GSK-2606414 (PERKi) is a potent and selective high affinity ligand of the PERK kinase, that interferes with kinase activity by competing for ATP [56,57]. In MHV-infected 17 Cl-1 cells at 5 and 8 h p.i., the drug prevented autophosphorylation of PERK (Fig 6A, lower panel) and phosphorylation of the PERK substrate, eIF2α, in a dose-dependent manner (Fig 6A, upper panel**),** effectively blocking this branch of the UPR. Pulse labelling of infected cells for one hour at 5 h p.i. revealed, as expected, that prevention of eIF2α phosphorylation increased modestly both viral (Fig 6A) and host protein synthesis (Fig 6B), without effect on mock-infected cells (Fig 6B). Also, analytical polysome profiling of MHV-infected cells treated with 5 μM of the PERKi for 5 h (Fig 6C) revealed a decrease in the accumulation of monosomes (80S) compared to MHV-infected cells at 5 h p.i. (Fig 5A, middle panel) showing a relief in translation inhibition. Despite the increased virus protein synthesis, 17 Cl-1 cell monolayers infected with MHV-A59 in the presence of the PERK inhibitor remarkably showed delayed formation of syncytia in comparison to untreated cells at 8 h p.i. (Fig 6D). The quantification of released virions through $TCID_{50}$ assays revealed an ~four-fold reduction in virus titre in cells incubated with PERKi compared to control cells (P= 0.0093; Fig 6E, left panel) whereas there was no difference in the quantification of intra- and extracellular virions in treated *versus* non-treated cells (Fig 6E, right panel). These observations suggest that relieving inhibition of protein synthesis – affecting both cellular and viral proteins – is detrimental to virus production and the development of syncytia in virus-infected cells.

Furthermore, we investigated how PERKi was affecting the different pathways of the UPR as a response to MHV infection. We monitored *BiP* at 5 h p.i. with different PERKi concentrations by qRT-PCR in three biological replicates. The ratio of *BiP* transcription to the house-keeping gene *Rpl19* was only slightly increased at the highest PERKi concentrations (Fig 6F, upper panel). Determination of *Xbp-1* splicing was carried out as earlier in MHV-infected cells at 5 h p.i. and treated with different PERKi concentration. *Xbp-1u* was the predominant form in mock-infected cells whereas *Xbp-1s* was the major species in MHV-infected cells in all cases (Fig 6F, lower

336 panel). These data indicate that the PERKi was very specific in inhibiting the PERK-eIF2α activity
337 but not the other branches of the UPR.
338
339 **Discussion:**
340
341 We have used ribosome profiling and parallel RNASeq to investigate changes in the cellular
342 translatome and transcriptome in response to infection with MHV, a representative of the
343 *Betacoronavirus* genus of the *Coronaviridae* family. These studies provide the highest resolution
344 data to date on the translatome of cells during coronavirus-induced stress.
345
346 RNASeq libraries revealed that some of the most significantly up-regulated cellular transcripts in
347 virus-infected cells were part of the UPR (*Herpud1* and *Chac1*) and changes in the translation
348 efficiency of cellular proteins were consistent with uORF-regulated responses to eIF2α
349 phosphorylation, including those previously implicated as effectors of the UPR such as *Atf4*, *Atf5*,
350 *Chop* and *Gadd34* [31-36,39]. These data confirm again that there is a close interplay between virus
351 infection and the UPR, with the host activating the UPR to combat the effects of virus infection, and
352 viruses sometimes manipulating the UPR to promote replication and pathogenesis [58-61]. The
353 intimate association of CoVs with the ER during replication results in ER stress responses as the
354 cell attempts to return to homeostasis [47, 62-66; reviewed in [67]).
355
356 The relative modulation of UPR branches differs between different CoVs [3,5,67]. For example,
357 SARS-CoV infection does not lead to *Xbp-1* splicing [47] whereas the IRE1 pathway is activated by
358 infectious bronchitis virus or MHV infection or by MHV S protein overexpression [27,68]. In spite
359 of the observed *Xbp-1* mRNA splicing during MHV infection [27], Xbp-1s protein had not
360 previously been detected in coronavirus-infected cells. In our study (5 and 8 h p.i. data sets), an

361 increased number of RPF reads mapped in the +2 reading frame of the *Xbp-1u* transcript
362 corresponding to translation of the *Xbp-1s* frameshifted isoform.
363
364 Activation of the ATF6 pathway by CoV infection has not yet been fully addressed. ATF6 cleavage
365 into its active form is observed during MHV infection but is significantly reduced at late time points
366 [27] although we could not detect the cleavage of this transcription factor by western blotting. In
367 addition, the trimmed ATF6 form is not detected in SARS-CoV infected cells [69]. Furthermore,
368 ER stress-responsive promoters exhibit little activity under these conditions. In the present study, an
369 induction of *BiP* transcription due to ATF6 activation was observed to a similar extent in both
370 tunicamycin-treated and MHV-infected cells, whereas BiP protein expression was only detected by
371 western blotting in tunicamycin-treated cells. Ribosome profiling data revealed that, in virus-
372 infected cells, the level of RPFs corresponding to the *BiP* CDS was not as high as in tunicamycin-
373 treated cells and this was probably the reason why this protein was not detected by western blot
374 analysis, although we can not rule out that BiP protein can be degraded as a response to MHV-
375 infection at a post-translational stage.
376
377 With respect to UPR-related inhibition mediated by eIF2α phosphorylation, it has been shown that
378 infectious bronchitis virus activates or suppresses protein kinase RNA-activated (PKR) and PERK
379 during the course of an infection [70] whereas transmissible gastroenteritis virus protein 7 emulates
380 the function of DNA damage-inducible protein 34 (GADD34) to dephosphorylate eIF2α [71]. Our
381 study reveals that MHV-A59 infection increases the level of p-eIF2α and ATF4 from 5 h p.i.
382 onwards. The RiboSeq data also revealed decreased translation of the *Atf4* uORF2 at 5 and 8 h p.i.
383 and a concomitant increase in translation of the main ORF. Although Bechill and colleagues [27]
384 failed to detect the products of ATF4 target genes, *Gadd34* and *Chop*, during MHV infection by
385 western blotting, we found evidence supporting an increase in translation of *Gadd34* and both
386 transcription and translation of *Chop* at later time points p.i.

We tested the effect of the selective PERK inhibitor GSK-2606414 on MHV replication [56,57]. GSK-2606414 (IC_{50} = 0.4 nM) exhibits >1000-fold selectivity for PERK over heme-regulated eIF2α (HR1) and PKR. Up to 5 μM of this inhibitor was well tolerated by 17 Cl-1 cells and, in MHV-infected cells, the prevention of eIF2α phosphorylation alleviated the inhibition in translation of cellular and viral proteins as expected. Surprisingly, the higher content of viral proteins did not lead to a more prominent cytopathic effect but instead delayed syncytia formation and reduced viral titre. Therefore, we conclude that UPR-mediated eIF2α phosphorylation may be favourable to MHV replication – perhaps by preventing translation of various anti-viral factors – and the pharmacological manipulation of this UPR branch can be explored as a potential target for antiviral intervention. Also, it will be interesting to investigate a potential additional role of this PERK inhibitor in the translocation of the spike (S) protein and in the regulation of the assembly of MHV-A59 particles.

Ribosome profiling provides information on initiating and elongating 80S ribosomes but (without modification) it does not report on free monosomes nor small subunits at early stages in initiation prior to formation of 80S complexes. Analytical polysome profiling showed an accumulation of 80S monosomes in MHV-infected cells from 5 h p.i. with the vast majority not being associated with mRNA which is a typical outcome of impaired translation [72]. This suggests that protein translation was inhibited at the stage of initiation probably due to the activation of the PERK branch in response to ER stress and the concomitant phosphorylation of eIF2α which can be alleviated by treating MHV infected cells with an specific PERK inhibitor. Phosphorylated eIF2α (p-eIF2α) forms a stable complex with eIF2B – the guanine exchange factor responsible for recycling inactive eIF2-GDP to eIF2-GTP – which rapidly reduces the pool of available eIF2B. This prevents recycling of the ternary complex of eIF2, GTP and Met-tRNAi and formation of the 43S pre-

initiation complex, and thus leads to a general shutdown of protein synthesis by inhibition of initiation [73].

Viruses commonly employ translational shutoff mechanisms to facilitate viral replication. On the one hand, shut-off of host cell translation can redirect the translation machinery towards viral gene expression if the virus has evolved non-canonical modes of translation, such as internal ribosome entry site (IRES) mediated initiation. On the other hand, the shut-off of host cell protein synthesis will inhibit a range of cellular anti-viral responses. Previous studies have shown that MHV can induce host translational shutoff and mRNA decay in LR7 cells with the concomitant formation of stress granules and processing bodies [26]. Furthermore, a number of reports have demonstrated that CoV nsp1, the most N-terminal product of the replicase polyprotein, modulates host protein synthesis. In different CoVs, nsp1 has been shown to associate with the 40S ribosomal subunit thus preventing viral and cellular mRNA translation; induce cellular mRNA degradation via an endonucleolytic mRNA cleavage in the 5′ region of capped mRNA; and selectively target nuclear host mRNAs and transport them to the cytoplasm for degradation [28-29,74-75]. The involvement of nsp1 in host protein translation could not be ruled out in this study without a comparison with a mutant virus lacking nsp1. However, the UPR-related translational modulation and the CoV nsp1-related modification of translation (and mRNA degradation) testify to the complexity of cellular translational shutoff mechanisms utilised by CoVs. How MHV proteins can be synthesised in a state of global translation inhibition has been the subject of previous speculation. Viral mRNAs contain a common 5′-leader sequence (65–90 nucleotides long) that could bind to the nucleocapsid (N) protein to form a complex that might act as a strong translation initiation signal [76], or the leader RNA sequence may bind to nsp1, protecting the viral mRNAs from nsp1-induced RNA cleavage [75,77]. However, we found previously that virus mRNAs 2–7 were translated with generally similar efficiencies during infection and, importantly, were not preferentially translated

437 relative to host mRNAs. Thus we concluded that the synthesis of large quantities of virus proteins,
438 especially N, was achieved mainly through high levels of transcription [16].

439

440 In conclusion, this study provides a survey of coronavirus effects on the cellular transcriptome and
441 translatome, complementing previous investigations on the UPR and host cell shutoff during MHV
442 infection. The results of our analyses will help inform further investigations on host-CoV
443 interactions and several differentially expressed genes identified may help identify new targets for
444 antiviral intervention.

445

446

Materials and Methods:

Cells and virus: Murine 17 clone 1 (17 Cl-1) ([82], a kind gift of Dr Stanley Sawicki, University of Toledo) cells were maintained in Dulbecco's modification of Eagle's medium supplemented with 10% (vol/vol) fetal calf serum (FCS). Recombinant MHV strain A59 (MHV-A59) was derived as previously described ([78], a kind gift of Dr Stanley Sawicki, University of Toledo, ATCC VR764). Upon reaching 70–80% confluence, 17 Cl-1 cells were infected with MHV-A59 at MOI 10 in infection medium [Hank's balanced salt solution (HBSS) containing 50 µg/ml DEAE-dextran and 0.2% bovine serum albumin (BSA)]. After 45 min at 37 ºC, the inoculum was removed and the cells were incubated in DMEM containing 10% FCS, 100 U/ml penicillin and 100 µg/ml streptomycin at 37 ºC until harvest.

For the tunicamycin experiments, 17 Cl-1 cells were incubated in the presence of tunicamycin (2 µg/ml). 17 Cl-1 mock and MHV-infected cells were treated with different concentrations (1–5 µM) of the PERK-inhibitor GSK-2606414 (PERKi), a kind gift of Dr Edward Emmott and Prof Ian Goodfellow. PERKi was added to the cells just after the adsorption time and maintained until cells were harvested.

Ribosomal profiling and RNASeq data: 17 Cl-1 cells were grown on 100-mm dishes to 90% confluency and infected with MHV-A59 at a multiplicity of infection (MOI) of 10. At indicated h p.i., cells were rinsed with 5 ml of ice-cold PBS, flash frozen in a dry ice/ethanol bath and lysed with 400 µl of lysis buffer [20 mM Tris-HCl pH 7.5, 150 mM NaCl, 5 mM $MgCl_2$, 1 mM DTT, 1% Triton X-100, 100 µg/ml cycloheximide and 25 U/ml TURBO DNase (Life Technologies)]. For the tunicamycin experiments, 17 Cl-1 cells were incubated in the presence of tunicamycin (2 µg/ml) and, after 6 h, cells were rinsed with 5 ml of ice-cold PBS and then flash frozen. The cells were scraped extensively to ensure lysis, collected and triturated ten times with a 26-G needle. Cell lysates were clarified by centrifugation at 13,000 g for 20 min at 4°C. Lysates were subjected to Ribo-Seq and RNA-Seq based on previously reported protocols [16,79]. Ribosomal RNA was

474 removed using Ribo-Zero Gold rRNA removal kit (Illumina) and library amplicons were
475 constructed using a small RNA cloning strategy adapted to Illumina smallRNA v2 to allow
476 multiplexing. Amplicon libraries were deep sequenced using an Illumina NextSeq500 platform.
477 Due to the very large amounts of vRNA produced during infection, mock samples were processed
478 separately from infected samples to avoid contamination. Ribo-Seq and RNA-Seq sequencing data
479 have been deposited in ArrayExpress (http://www.ebi.ac.uk/arrayexpress) under the accession
480 numbers E-MTAB-5391 and E-MTAB-6278.
481
482 **Computational analysis of RiboSeq and RNASeq data:** Reads were trimmed for adaptor
483 sequences, filtered for length $\geq$ 25 nt, and reads mapping to *Mus musculus* rRNA (downloaded from
484 SILVA database) or MHV-A59 viral RNA (AY700211.1) (with up to 2 mismatches) removed, as
485 previously described [16]. The remaining reads were aligned directly to the mouse genome (FASTA
486 and GTF gencode release M20, GRCm38, primary assembly) (with up to 2 mismatches) using
487 STAR (parameters: --outFilterIntronMotifs RemoveNoncanonicalUnannotated --
488 outMultimapperOrder Random) [80]. Reads on protein-coding genes were tabulated using htseq-
489 count (version 0.9.1), covering the whole gene for differential transcription analysis (parameters: -a
490 0 -m union -s yes -t gene) and just the CDS for the translation efficiency analysis (parameters:
491 htseq-count -a 0 -m intersection-strict -s yes -t CDS) , using the GTF file from the above gencode
492 release as the gene feature annotation [81]. Thus the differential TE analysis excludes reads
493 mapping to uORFs or non-annotated coding sequences (unless such sequences overlap the main
494 annotated ORF).
495
496 Differential transcription analysis was performed using DESeq2 (version 1.18.1) [21] and
497 translation efficiency analysis with Xtail (version 1.1.5) [29]. For each analysis, low count genes
498 (with fewer than ten counts from all samples combined) were discarded, following which read
499 counts were normalised by the total number of reads mapping to host mRNA for that library. This

means the very large amount of vRNA present in infected samples should not affect the analyses. Shrinkage of the transcriptional fold changes to reduce noise in lowly-expressed genes was applied using lfcShrink (parameter: type='normal').

A given gene was considered to be differentially expressed if the FDR was less than 0.05 and the fold change between the averages of infected and mock replicates was greater than two. Volcano plots and transcription vs TE comparison plots were generated using standard R plotting features and FDR and $\log_2$(fold change) values from the DESeq2 and Xtail analyses. All reported *p* values are corrected for multiple testing, though it's important to note the fold changes plotted in the transcription vs TE comparison are not filtered for significant *p* values before plotting.

To make the plots of RNASeq and RPF profiles for specific transcripts, reads were mapped to the specified transcript from the NCBI genome assembly using bowtie [82] allowing two mismatches (parameters: -v 2, --best). Coordinates for known uORFs were taken from the literature and the positions of start and stop codons in all frames determined. Read density (normalised by total reads mapping to host mRNA for each library, to give reads per million mapped reads) was calculated at each nucleotide on the transcript and plotted, according to phase. Read positions were offset by +12 nt so that plotted data represent the position of the ribosomal P site. Bar widths were increased to 4nt to aid visibility and were plotted on top of each other starting from the 5' end of the transcript.

Gene ontology and Reactome pathway enrichment analyses: Lists of gene IDs of significantly differentially expressed genes (Supplementary Table 1) were used for GO term enrichment analysis by the PANTHER web server under the default conditions (release 20190606, GO database released 2019-02-02) [83], against a background list of all the genes that passed the threshold for inclusion in that expression analysis. For Reactome pathway enrichment (version 69) [49], the same

differentially expressed gene lists were converted to their human orthologues and analysed using the reactome.org web server to determine which pathways are significantly over-represented.

Enrichment analysis for eIF2α-phosphorylation-resistant genes:

A list of genes reported resistant to translational repression by p-eIF2α was constructed based on Andreev et al., 2015 [36] and references within (excluding those from IRESite, which were not found eIF2α-resistant in their study). Mouse homologues of these genes were identified using NCBI homologene database. Enrichment of genes in this pathway amongst the genes with significantly increased translational efficiency, compared to a background of all *Mus musculus* genes included in the TE analysis with any GO annotation, was calculated using a Fisher Exact test.

Quantitative real-time PCR assays: Total RNA was isolated as described previously [79] for RNA-Seq analysis, and cDNA was synthesised from 1 µg total RNA. Transcript levels were determined by quantitative real-time PCR using a Rotor-Gene 3000 (Corbett Research). Reactions were performed in a final volume of 20 µl containing Hot Start Taq (1 U; QIAGEN), 3.5 mM $MgCl_2$, 2.5 mM deoxynucleotides, SYBR Green dye, 500 nM forward and reverse specific primers and 1 µl of cDNA. After enzyme activation (95 °C, 15 min), amplification was carried out in a three-step PCR procedure (50 cycles: 15 s at 95 °C for denaturation, 20 s at 55 ºC for annealing and 20 s at 72 °C for extension). Non-template controls were included for each primer pair, and each PCR reaction was carried out in triplicate.

Immunoblotting: Proteins were separated by 10% or 12% SDS-PAGE and transferred to nitrocellulose membranes. These were blocked (5% non-fat milk powder in PBST [137 mM NaCl, 2.7 mM KCl, 10 mM Na_2HPO_4, 1.5 mM KH_2PO_4, pH 6.7, and 0.1% Tween 20]) and probed with mouse monoclonal antibodies raised against N (1:1,000), S (1:500) - kind gifts of Dr Helmut Wege, University of Würzburg -, GAPDH (G8795, Sigma-Aldrich, 1:20,000), S6 (1:500, Cell Signaling);

551 rabbit monoclonal antibodies against BiP (1:1,000, Abcam) and RPL10a (1:500, Abcam); or
552 polyclonal rabbit anti-ATF4 (1:500, Proteintech), anti-eIF2α, anti-p(Ser-51)-eIF2α (1:1,000, Cell
553 Signaling) and anti-PERK (1:1000, Abcam). Membranes were incubated in the dark with an IRDye-
554 conjugated secondary antibody in phosphate-buffered saline (PBS) and 0.1% Tween 20 [IRDye
555 800CW Donkey Anti-Mouse IgG (H+L), IRDye 800CW Donkey Anti-Rabbit IgG (H+L), IRDye
556 680RD Goat Anti-Mouse IgG (H+L) and IRDye 680RD Goat Anti-Mouse IgM (μ chain specific)].
557 Blots were scanned using an Odyssey Infrared Imaging System (Licor).
558
559 **Polysome profiling:** 17 Cl-1 cells were infected as previously described. Ten minutes prior to
560 harvesting, cells were treated with cycloheximide (100 μg/ml), washed with PBS and lysed in a
561 buffer containing 20 mM Tris HCl pH 7.5, 100 mM KCl, 5 mM MgOAc, 0.375 mM CHX, 1 mM
562 DTT, 0.1 mM PMSF, 2U/μl DNase I, 0.5% NP-40, supplemented with protease and phosphatase
563 inhibitors (ThermoFisher Scientific). Following trituration with a 26-G needle (ten passes), lysates
564 were cleared (13,000 *g* at 4 ºC for 20 min) and the supernatants layered onto 12 mL sucrose density
565 gradients (10–50% sucrose in TMK buffer – 20 mM Tris-HCl pH 7.5, 100 mM KCl, 5 mM $MgCl_2$)
566 prepared in Beckman SW41 polypropylene tubes using a Gradient Master (Biocomp). Following
567 centrifugation (200,000 *g* for 90 min at 4 ºC), fractions were prepared using an ISCO fractionator
568 monitoring absorbance at 254 nm. Proteins were concentrated from fractions using methanol-
569 chloroform extraction [84] and subjected to immunoblotting analysis. Polysome profiling in higher
570 salt conditions was carried out as described above except that the lysis buffer and sucrose density
571 gradient contained 400 mM KCl.
572
573 **Metabolic labelling:** 17 Cl-1 cell monolayers were infected with MHV A-59 at a MOI of 10
574 PFU/cell. At 5 h p.i., cells were washed twice with PBS and labelled for 1 h in methionine-free
575 DMEM supplemented with 125 μCi/ml [^{35}S] methionine. After this period, cells were harvested,
576 washed twice with PBS and resuspended in lysis buffer (50 mM Tris pH 7.5, 100 mM NaCl, 5 mM

577 EDTA, 0.5% NP40). Cell lysate aliquots were mixed with Laemmli's sample buffer to a final
578 concentration of 1× and subjected to 10% SDS-PAGE followed by autoradiography.
579
580 **$TCID_{50}$ assays:** Virus replication was assessed using a 50% tissue culture infective dose ($TCID_{50}$)
581 assay. One day prior to infection, 17 Cl-1 cells were seeded in 96-well plates at 4×10^3 cells/well in
582 a final volume of 100 µl/well. Supernatant derived from extracellular media (released virions) or
583 from extracellular media and cells subjected to a cycle of freezing/thawing (intra- and extracelluar
584 virions) was harvested at 6 h p.i. from a six-well plate infected with MHV-A59 in the presence or
585 absence of PERKi, and serially diluted 10-fold in infection medium. At 18 h p.i., cells were washed
586 with PBS, fixed with formal saline and stained with 0.1% toluidine blue. Wells showing any sign of
587 cytopathic effect (CPE) were scored as positive. Experiments were conducted using triplicate
588 biological repeats, each diluted in parallel and used to infect eight rows of wells. For each biological
589 repeat, the 50% endpoint titre was calculated according to the method of Reed and Muench [85].
590
591

592 **References:**

593 1. Channappanavar R, Perlman S (2017) Pathogenic human coronavirus infections: causes and
594 consequences of cytokine storm and immunopathology. Semin Immunopathol. doi:
595 10.1007/s00281-017-0629-x.
596
597 2. Walsh D, Mathews MB, Mohr I (2013) Tinkering with translation: protein synthesis in virus-
598 infected cells. Cold Spring Harb Perspect Biol 5:a012351.
599
600 3. Fung TS, Liu DX (2014) Coronavirus infection, ER stress, apoptosis and innate immunity. Front
601 Microbiol 5: 296.
602
603 4. Ron D, Walter P (2007) Signal integration in the endoplasmic reticulum unfolded protein
604 response. Nat Rev Mol Cell Biol 8: 519-529.
605
606 5. Fung TS, Liao Y, Liu DX (2016) Regulation of stress responses and translational control by
607 coronavirus. Viruses 8: E184.
608
609 6. Ingolia NT, Ghaemmaghami S, Newman JR, Weissman JS (2009) Genome-wide analysis in vivo
610 of translation with nucleotide resolution using ribosome profiling. Science 324: 218-223.
611
612 7. Ingolia NT, Lareau LF, Weissman JS (2011) Ribosome profiling of mouse embryonic stem cells
613 reveals the complexity and dynamics of mammalian proteomes. Cell 147: 789-802.
614
615 8. Ingolia NT (2014) Ribosome profiling: new views of translation, from single codons to genome
616 scale. Nat Rev Genet 15: 205-213.
617
618 9. Stern-Ginossar N, Weisburd B, Michalski A, Le VT, Hein MY, Huang SX, Ma M, Shen B, Qian
619 SB, Hengel H, et al (2012) Decoding human cytomegalovirus. Science 338: 1088-1093.
620
621 10. Liu X, Jiang H, Gu Z, Roberts, JW (2013) High-resolution view of bacteriophage lambda gene
622 expression by ribosome profiling. Proc Natl Acad Sci U S A 110: 11928-11933.
623
624 11. Arias C, Weisburd B, Stern-Ginossar N, Mercier A, Madrid AS, Bellare P, Holdorf M,
625 Weissman JS, Ganem D (2014) KSHV 2.0: a comprehensive annotation of the Kaposi's sarcoma-
626 associated herpesvirus genome using next-generation sequencing reveals novel genomic and
627 functional features. PLoS Pathog 10: e1003847.
628
629 12. Rutkowski AJ, Erhard F, L'Hernault A, Bonfert T, Schilhabel M, Crump C, Rosenstiel P,
630 Efstathiou S, Zimmer R, Friedel CC, et al (2015) Widespread disruption of host transcription
631 termination in HSV-1 infection. Nat Commun 6: 7126.
632
633 13. Tirosh O, Cohen Y, Shitrit A, Shani O, Le-Trilling VT, Trilling M, Friedlander G, Tanenbaum
634 M, Stern-Ginossar N (2015) The transcription and translation landscapes during human
635 cytomegalovirus infection reveal novel host-pathogen interactions. PLoS Pathog 11: e1005288.
636
637 14. Yang Z, Cao S, Martens CA, Porcella SF, Xie Z, Ma M, Shen B, Moss B (2015) Deciphering
638 poxvirus gene expression by RNA sequencing and ribosome profiling. J Virol 89: 6874-6886.
639
640 15. Bercovich-Kinori A, Tai J, Gelbart IA, Shitrit A, Ben-Moshe S, Drori Y, Itzkovitz S,
641 Mandelboim M, Stern-Ginossar N (2016) A systematic view on influenza induced host shutoff.
642 Elife 5: e18311.

16. Irigoyen N, Firth AE, Jones JD, Chung BY, Siddell SG, Brierley I (2016) High-resolution analysis of coronavirus gene expression by RNA sequencing and ribosome profiling. PLoS Pathog 12: e1005473.

17. Dai A, Cao S, Dhungel P, Luan Y, Liu Y, Xie Z, Yang Z (2017) Ribosome profiling reveals translational upregulation of cellular oxidative phosphorylation mRNAs during vaccinia virus-induced host shutoff. J Virol 91: e01858.16.

18. Irigoyen N, Dinan AM, Brierley I, Firth AE (2018) Ribosome profiling of the retrovirus murine leukemia virus. Retrovirology 15: 10.

19. Reid DW, Campos RK, Child JR, Zheng T, Chan KWK, Bradrick SS, Vasudevan SG, Garcia-Blanco MA, Nicchitta CV (2018) Dengue virus selectively annexes endoplasmic reticulum-associated translation machinery as a strategy for co-opting host cell protein synthesis. J Virol 92:e01766-17.

20. Gerashchenko MV, Gladyshev VN (2014) Translation inhibitors cause abnormalities in ribosome profiling experiments. Nucleic Acids Res 42(17):e134.

21. Love MI, Huber W, Anders S (2014) Moderated estimation of fold change and dispersion for RNA-seq data with DESeq2. Genome Biol 15(12):550.

22. Hollien J, Weissman JS (2006) Decay of endoplasmic reticulum-localized mRNAs during the unfolded protein response. Science 313: 104-107.

23. Hiramatsu N, Joseph VT, Lin JH (2011) Monitoring and manipulating mammalian unfolded protein response. Methods Enzymol 491: 183-198.

24. Siddell SG, Wege H, Barthel, A, ter Meulen V (1980) Coronavirus JHM: cell-free synthesis of structural protein p60. J Virol 33: 10-17.

25. Hilton A, Mizzen L, MacIntyre G, Cheley S, Anderson R (1986) Translational control in murine hepatitis virus infection. J Gen Virol 67: 923-932.

26. Raaben M, Groot Koerkamp MJ, Rottier PJ, de Haan CA (2007) Mouse hepatitis coronavirus replication induces host translational shutoff and mRNA decay, with concomitant formation of stress granules and processing bodies. Cell Microbiol 9: 2218-2229.

27. Bechill J, Chen Z, Brewer JW, Baker SC (2008) Coronavirus infection modulates the unfolded protein response and mediates sustained translational repression. J Virol 82: 4492-4501.

28. Kamitani W, Huang C, Narayanan K, Lokugamage KG, Makino S (2009) A two-pronged strategy to suppress host protein synthesis by SARS coronavirus Nsp1. Nat Struct Mol Biol 16: 1134-1140.

29. Lokugamage KG, Narayanan K, Nakagawa K, Terasaki K, Ramirez SI, Tseng CT, Makino S (2015) Middle east respiratory syndrome coronavirus nsp1 inhibits host gene expression by selectively targeting mRNAs transcribed in the nucleus while sparing mRNAs of cytoplasmic origin. J Virol 89: 10970-10981.

30. Xiao Z, Zou Q, Liu Y, Yang X (2016) Genome-wide assessment of differential translations with ribosome profiling data. Nat Commun 7: 11194.

31. Lu PD, Harding HP, Ron D (2004) Translation reinitiation at alternative open reading frames regulates gene expression in an integrated stress response. J Cell Biol 167: 27-33.

32. Vattem KM, Wek RC (2004) Reinitiation involving upstream ORFs regulates ATF4 mRNA translation in mammalian cells. Proc Natl Acad Sci U S A 101: 11269-11274.

33. Watatani Y, Ichikawa K, Nakanishi N, Fujimoto M, Takeda H, Kimura N, Hirose H, Takahashi S, Takahashi Y (2008) Stress-induced translation of ATF5 mRNA is regulated by the 5´-untranslated region. J Biol Chem 283: 2543-2553.

34. Zhou D, Palam LR, Jiang L, Narasimhan J, Staschke KA, Wek RC (2008) Phosphorylation of eIF2 directs ATF5 translational control in response to diverse stress conditions. J Biol Chem 283: 7064-7073.

35. Palam LR, Baird TD, Wek RC (2011) Phosphorylation of eIF2 facilitates ribosomal bypass of an inhibitory upstream ORF to enhance CHOP translation. J Biol Chem 286: 10939-10949.

36. Andreev DE, O'Connor PB, Fahey C, Kenny EM, Terenin IM, Dmitriev SE, Cormican P, Morris DW, Shatsky IN, Baranov PV (2015) Translation of 5´leaders is pervasive in genes resistant to eIF2 repression. Elife 4: e03971.

37. Brush MH, Weiser DC, Shenolikar S (2003) Growth arrest and DNA damage-inducible protein GADD34 targets protein phosphatase 1 alpha to the endoplasmic reticulum and promotes dephosphorylation of the alpha subunit of eukaryotic translation initiation factor 2. Mol Cell Biol 23(4):1292-303.

38. Novoa I, Zeng H, Harding HP, Ron D (2001) Feedback inhibition of the unfolded protein response by GADD34-mediated dephosphorylation of eIF2alpha. J Cell Biol 28;153(5):1011-22.

39. Lee YY, Cevallos RC, Jan E (2009) An upstream open reading frame regulates translation of GADD34 during cellular stresses that induce eIF2alpha phosphorylation. J Biol Chem 284(11):6661-73.

40. Mungrue IN, Pagnon J, Khannim O, Gargalovic PS, Lusis AJ (2009) CHAC1/MGC4504 is a novel proapoptotic component of the unfolded protein response, downstream of the ATF4-ATF3-CHOP cascade. J Immunol 1;182(1):466-76.

41. Yamamoto K, Yoshida H, Kokame K, Kaufman RJ, Mori K (2004) Differential contributions of ATF6 and XBP1 to the activation of endoplasmic reticulum stress-responsive cis-acting elements ERSE, UPRE and ERSE-II. J Biochem 136(3):343-50.

42. Baumeister P, Luo S, Skarnes WC, Sui G, Seto E, Shi Y, Lee AS (2005) Endoplasmic reticulum stress induction of the Grp78/BiP promoter: activating mechanisms mediated by YY1 and its interactive chromatin modifiers. Mol Cell Biol. 25(11):4529-40.

43. Yoshida H, Matsui T, Yamamoto A, Okada T, Mori K (2001) XBP1 mRNA is induced by ATF6 and spliced by IRE1 in response to ER stress to produce a highly active transcription factor. Cell 28: 881-891.

746 44. Nishitoh H (2012) CHOP is a multifunctional transcription factor in the ER stress response. J
747 Biochem 151(3):217-9.
748
749 45. Ma Y, Hendershot LM (2003) Delineation of a negative feedback regulatory loop that controls
750 protein translation during endoplasmic reticulum stress. J Biol Chem 278(37):34864-73.
751
752 46. Jiang XS, Tang LY, Dai J, Zhou H, Li SJ, Xia QC, Wu JR, Zeng R (2005) Quantitative analysis
753 of severe acute respiratory syndrome (SARS)-associated coronavirus-infected cells using proteomic
754 approaches: implications for cellular responses to virus infection. Mol Cell Proteomics 4: 902-913.
755
756 47. Versteeg GA, van de Nes PS, Bredenbeek PJ, Spaan WJ (2007) The coronavirus spike protein
757 induces endoplasmic reticulum stress and upregulation of intracellular chemokine mRNA
758 concentrations. J Virol 81: 10981-10990.
759
760 48. Yeung YS, Yip CW, Hon CC, Chow KY, Ma IC, Zeng F, Leung FC (2008) Transcriptional
761 profiling of Vero E6 cells over-expressing SARS-CoV s2 subunit: insights on viral regulation of
762 apoptosis and proliferation. Virology 371: 32-43.
763
764 49. Fabregat A, Sidiropoulos K, Viteri G, Forner O, Marin-Garcia P, Arnau V, D'Eustachio P, Stein
765 L, Hermjakob H (2017) Reactome pathway analysis: a high-performance in-memory approach.
766 BMC Bioinformatics 18(1):142.
767
768 50. Calfon M, Zeng H, Urano F, Till JH, Hubbard SR, Harding HP, Clark SG, Ron D (2002) IRE1
769 couples endoplasmic reticulum load to secretory capacity by processing the XBP-1 mRNA. Nature
770 415: 92-96.
771
772 51. Ye J, Rawson RB, Komuro R, Chen X, Davé UP, Prywes R, Brown MS, Goldstein JL (2000)
773 ER stress induces cleavage of membrane-bound ATF6 by the sames proteases that process SREBPs.
774 Mol Cell 6: 1355-1364.
775
776 52. Haze K, Yoshida H, Yanagi H, Yura U, Mori K (1999) Mammalian transcription factor ATF6 is
777 synthesized as a transmembrane protein and activated by proteolysis in response to endoplasmic
778 reticulum stress. Mol Biol Cell 10:3787-3799.
779
780 53. Harding HP, Zhang Y, Ron D (1999) Protein translation and folding are coupled by an
781 endoplasmic-reticulum-resident kinase. Nature 397: 271-274.
782
783 54. Harding HP, Zhang Y, Bertolotti A, Zeng H, Ron D (2000) Perk is essential for translational
784 regulation and cell survival during the unfolded protein response. Mol Cell 5: 897-904.
785
786 55. Harding HP, Novoa I, Zhang Y, Zeng H, Wek R, Schapira M, Ron D (2000) Regulated
787 translation initiation controls stress-induced gene expression in mammalian cells. Mol Cell 6: 1099-
788 1108.
789
790 56. Axten JM, Medina JR, Feng Y, Shu A, Romeril SP, Grant SW, Li WH, Heerding DA, Minthorn
791 E, Mencken T, Atkins C, Liu Q, Rabindran S, Kumar R, Hong X, Goetz A, Stanley T, Taylor JD,
792 Sigethy SD, Tomberlin GH, Hassell AM, Kahler KM, Shewchuk LM, Gampe RT (2012) Discovery
793 of 7-methyl-5-(1-{[3-(trifluoromethyl)phenyl]acetyl}-2,3-dihydro-1H-indol-5-yl)-7H-pyrrolo[2,3-
794 d]pyrimidin-4-amine (GSK2606414), a potent and selective first-in-class inhibitor of protein kinase
795 R (PKR)-like endoplasmic reticulum kinase (PERK). J Med Chem *55*, 7193-7207.
796

797 57. Harding HP, Zyryanova AF, Ron D (2012) Uncoupling proteostasis and development in vitro
798 with a small molecule inhibitor of the pancreatic endoplasmic reticulum kinase, PERK. J Biol Chem
799 *287*, 44338-44344.
800
801 58. Lazar C, Uta M, Branza-Nichita N (2014) Modulation of the unfolded protein response by the
802 human hepatitis B virus. Front Microbiol 5: 433.
803
804 59. Carpenter JE, Grose C (2014) Varicella-zoster glycoprotein expression differentially induces the
805 unfolded protein response in infected cells. Front Microbiol 5: 322.
806
807 60. Chan SW (2014) The unfolded protein response in virus infections. Front Microbiol 5: 518.
808
809 61. Perera N, Miller JL, Zitzmann N (2017) The role of the unfolded protein response in dengue
810 virus pathogenesis. Cell Microbiol 19: doi: 10.1111/cmi.12734
811
812 62. David-Ferreira JF, Manaker RA (1965) An electron microscopy study of the development of a
813 mouse hepatitis virus in tissue culture cells. J Cell Biol 24: 57-78.
814
815 63. Klumperman J, Locker JK, Meijer A, Horzinek MC, Geuze HJ, Rottier PJ (1994) Coronavirus
816 M proteins accumulate in the Golgi complex beyond the site of virion budding. J Virol 68: 6523-
817 6534.
818
819 64. Stertz S, Reichelt M, Spiegel M, Kuri T, Martínez-Sobrido L, García-Sastre A, Weber F, Kochs
820 G (2007) The intracellular sites of early replication and budding of SARS-coronavirus. Virology
821 361: 304-315.
822
823 65. Reggiori F, Monastyrska I, Verheije MH, Calì T, Ulasli M, Bianchi S, Bernasconi R, de Haan
824 CA, Molinari M (2010) Coronaviruses hijack the LC3-I-positive EDEMosomes, ER-derived
825 vesicles exporting short-lived ERAD regulators, for replication. Cell Host Microbe 7: 500-508.
826
827 66. Maier HJ, Hawes PC, Cottam EM, Mantell J, Verkade P, Monaghan P, Wileman T, Britton P
828 (2013) Infectious bronchitis virus generates spherules from zippered endoplasmic reticulum
829 membranes. MBio 4: e00801-13.
830
831 67. Fung TS, Liao Y, Liu DX (2014) The endoplasmic reticulum stress sensor IREa protects cells
832 from apoptosis induced by the coronavirus infectious bronchitis virus. J Virol 88: 12752-12764.
833
834 68. Fung TS, Huang M, Liu DX (2014) Coronavirus-induced ER stress response and its
835 involvement in regulation of coronavirus-host interactions. Virus Res 194: 110-123.
836
837 69. DeDiego ML, Nieto-Torres JL, Jiménez-Guardeño JM, Regla-Nava JA, Alvarez E, Oliveros JC,
838 Zhao J, Fett C, Perlman S, Enjuanes L (2011) Severe acute respiratory syndrome coronavirus
839 envelope protein regulates cell stress response and apoptosis. PLoS Pathog 7: e1002315.
840
841 70. Liao Y, Fung TS, Huang M, Fang SG, Zhong Y, Liu DX (2013) Upregulation of
842 CHOP/GADD153 during coronavirus infectious bronchitis virus infection modulates apoptosis by
843 restricting activation of the extracellular signal-regulated kinase pathway. J Virol 87: 8124-8134.
844
845 71. Cruz JL, Sola I, Becares M, Alberca B, Plana J, Enjuanes L, Zuñiga S (2011) Coronavirus gene
846 7 counteracts host defenses and modulates virus virulence. PLoS Pathog 7: e1002090.
847

72. Brina D, Grosso S, Miluzio A, Biffo S (2011) Translational control by 80S formation and 60S availability: the central role of eIF6, a rate limiting factor in cell cycle progression and tumorigenesis. Cell Cycle *10*, 3441-3446.

73. Hinnebusch AG (2014) The scanning mechanism of eukaryotic translation initiation. Annu Rev Biochem *83*, 779-812.

74. Kamitani W, Narayanan K, Huang C, Lokugamage K, Ikegami T, Ito N, Kubo H, Makino S (2006) Severe acute respiratory syndrome coronavirus nsp1 protein suppresses host gene expression by promoting host mRNA degradation. Proc Natl Acad Sci U S A 103: 12885-12890.

75. Huang C, Lokugamage KG, Rozovics JM, Narayanan K, Semler BL, Makino S (2011) SARS coronavirus nsp1 protein induces template-dependent endonucleolytic cleavage of mRNAs: viral mRNAs are resistant to nsp1-induced RNA cleavage. PLoS Pathog 7: e1002433.

76. Tahara SM, Dietlin TA, Bergmann CC, Nelson GW, Kyuwa S, Anthony RP, Stohlman SA (1994) Coronavirus translational regulation: leader affects mRNA efficiency. Virology 202: 621-630.

77. Tanaka T, Kamitani W, DeDiego ML, Enjuanes L, Matsuura Y (2012) Severe acute respiratory syndrome coronavirus nsp1 facilitates efficient propagation in cells through a specific translational shutoff of host mRNA. J Virol 86: 11128-11137.

78. Coley SE, Lavi E, Sawicki SG, Fu L, Schelle B, Karl, N, Siddell SG, Thiel V (2005) Recombinant mouse hepatitis virus strain A59 from cloned, full-length cDNA replicates to high titers in vitro and is fully pathogenic *in vivo*. J Virol 79: 3097-3106.

79. Chung BY, Hardcastle TJ, Jones JD, Irigoyen N, Firth AE, Baulcombe DC, Brierley I (2015) The use of duplex-specific nuclease in ribosome profiling and a user-friendly software package for Ribo-seq data analysis. RNA 21: 1731-1745.

80. Dobin A, Davis CA, Schlesinger F, Drenkow J, Zaleski C, Jha S, Batut P, Chaisson M, Gingeras TR (2013) STAR: ultrafast universal RNA-seq aligner. Bioinformatics 1;29(1):15-21.

81. Anders S, Pyl PT, Huber W (2015) HTSeq - a Python framework to work with high-throughput sequencing data. Bioinformatics 31: 166-169.

82. Langmead B, Trapnell C, Pop M, Salzberg SL (2009) Ultrafast and memory-efficient alignment of short DNA sequences to the human genome. Genome Biol 10(3):R25.

83. Mi H, Muruganujan A, Huang X, Ebert D, Mills C, GuoX, Thomas PD (2019) Protocol Update for large-scale genome and gene function analysis with the PANTHER classification system (v.14.0). Nat Protoc 14(3):703-721.

84. Eckert EA (1966) Envelope protein(s) derived from influenza virus. J Bacteriol 91: 1907-1910.

85. Reed LJ, Muench H. (1938). A simple method of estimating fifty percent endpoints. Am. J. Epidemiol. *27*, 493–497.

899 **Figure Captions:**
900
901 **Figure 1: Effect of MHV infection on cellular transcription. (A)** Volcano plot showing the
902 relative change in abundance of cellular transcripts and the FDR-corrected *p* value for differential
903 expression between the mock and infected samples. Grey vertical lines indicate a transcript
904 abundance fold change of 2. Genes which have fold changes greater than this threshold and a *p*
905 value of less than 0.05 are considered significantly differentially expressed and coloured orange if
906 up-regulated and blue if down-regulated. Selected genes are annotated in red and *Rpl19*, a
907 housekeeping gene, in yellow. **(B)** GO terms associated with the lists of differentially expressed
908 genes were determined. GO terms which are significantly enriched compared to a background of
909 GO terms associated with all genes detected in the differential transcription analysis are plotted.
910 Results associated with up-regulated gene list are in orange, down-regulated in blue. To avoid
911 redundancy, only the most specific GO term from each hierarchical cluster (determined by
912 PANTHER [80]) is plotted here, with only the top 20 enriched clusters plotted for the up-regulated
913 gene list. The GO term "response to topologically incorrect protein" is within the cluster "response
914 to unfolded protein". Only results with a *p* value of less than 0.05 are plotted, ranked by $\log_2$(fold
915 enrichment). Full results, including GO IDs, are in Supplementary Table 2. **(C)** Quantitative real-
916 time PCR (qRT-PCR) of selected up- (left panel) and down- (middle panel) regulated mRNAs in
917 three biological replicates of mock- and MHV-infected cells at 5 h p.i. Levels were normalised to
918 ribosomal protein L19 (*Rpl19*) transcript.
919
920 **Figure 2: Effects of MHV infection on translational efficiency (TE). (A)** Volcano plot showing
921 the relative change in TE of cellular transcripts, and the FDR-corrected *p* value, between the mock
922 and infected samples. Grey vertical lines indicate a fold change of 2. Genes which have fold
923 changes greater than this threshold and a *p* value of less than 0.05 are considered significantly
924 differentially translated and coloured orange if up-regulated and blue if down-regulated. Selected
925 genes are annotated in red and mentioned in the article text, except for the metabolism-related genes

926 *Ldha* – lactate dehydrogenase A, and *Uqcrq* - ubiquinol-cytochrome c reductase, complex III
927 subunit VII. **(B)** Plot of $\log_2$(fold changes) of TE vs transcript abundance for all genes included in
928 both analyses. Grey lines indicate fold changes of 2. Fold changes are plotted without filtering for
929 significant *p* values. Selected genes from each section are marked: genes up-regulated solely by
930 either transcription or TE are marked in blue (upper middle and right middle sections), genes down-
931 regulated solely by either transcription or TE are marked in red (lower middle and left middle
932 sections), genes which are 'buffered' by having opposing changes in transcription and TE are in
933 black (top left and bottom right sections), and C*hop*, which is up-regulated at the level of both
934 transcription and TE, is marked in green (top right section).
935
936 **Figure 3: Effect of MHV infection on unfolded protein response IRE 1α and ATF6 activity.** 17
937 Cl-1 cells were incubated in the presence of tunicamycin (2 µg/ml) or infected with MHV-A59
938 (MOI 10) and harvested at 2.5, 5, 8 and 10 h p.i. (**A**) RT-PCR analysis of *Xbp-1u* and *Xbp-1s*
939 mRNAs. Total RNA (1µg) was subjected to RT-PCR analysis using primers flanking the *Xbp-1*
940 splice site. PCR products were resolved in a 3% TBE-agarose gel and visualised by ethidium
941 bromide staining. *Rpl19* RT-PCR product was used as a loading control. Molecular size markers
942 (nt) are indicated on the left. Note as gel loads are normalised by total RNA concentration, Xbp-1
943 mRNA levels appear to diminish at late timepoints in samples from MHV infected cells, as the
944 increased viral RNA levels decrease the relative proportion of Xbp-1 transcripts in the load. (**B**)
945 Analysis of RPFs (mock and MHV-infected samples plus tunicamycin-treated sample) and
946 RNASeq (mock and MHV-infected samples) mapping to *Xbp-1u* (NCBI RefSeq mRNA
947 NM_013842). Cells harvested by flash-freezing. Reads are plotted at the inferred position of the
948 ribosomal P site (calculated based on the position of the 5 end of the read) and coloured according
949 to the frame of translation: pink for 0-frame, blue for +1, yellow for +2. The 5´ end position of
950 RNASeq reads is not determined by ribosome position and therefore should not show a dominant
951 frame. The main ORF (0 frame) is shown at the top in pink, with start and stop codons in all three

frames marked by green and red bars (respectively) in the three panels below. The yellow rectangle in the +2 frame indicates the extended ORF in *Xbp-1s* and reads resulting from translation of this spliced isoform can be seen in yellow (+2 frame), downstream of the main ORF annotated stop codon. Dotted lines serve as markers for the start and end of the features in their matching colour. Note that read densities are plotted as reads per million host-mRNA-mapping reads, and that bar widths were increased to 4-nt to aid visibility and were plotted on top of each other starting from the 5' end of the transcript. (**C**) qRT-PCR of three biological replicates of *BiP* transcripts normalised by *Rpl19* transcript. Note that the *BiP/Rpl19* transcription ratio is the one plotted. (**D**) Cell lysates were analysed by 12% SDS-PAGE and immunoblotted using anti-BiP and anti-N antibodies (green fluorescent secondary antibody). GAPDH was used as a loading control (red fluorescent secondary antibody). Molecular masses (kDa) are indicated on the left.

Figure 4: Effect of MHV infection on unfolded protein response PERK-eIF2α-ATF4 activity. 17 Cl-1 cells were incubated in the presence of tunicamycin (2 µg/ml) or infected with MHV-A59 (MOI 10) and harvested at 2.5, 5, 8 and 10 h p.i. (**A**) qRT-PCR of three biological replicates of *Chop* transcripts normalised by *Rpl19* transcript. Note that the *Chop/Rpl19* transcription ratio is the one plotted. (**B**) Cell lysates were separated by 12% SDS-PAGE and immunoblotted using anti-ATF4, anti-p-eIF2α, anti-eIF2α, anti-PERK and anti-N antibodies (green fluorescent secondary antibody). GAPDH was used as a loading control (red fluorescent secondary antibody). Molecular masses (kDa) are indicated on the left. (**C**) Analysis of RPFs (mock and MHV-infected samples plus tunicamycin-treated sample) and RNASeq (mock and MHV-infected samples) mapping to *Atf4* (NCBI RefSeq mRNA NM_009716). Plot constructed as described for Fig 3D but with yellow rectangles in the +2 frame here representing the *Atf4* uORFs.

Figure 5: Polysome profiling of 17 Cl-1 cells infected with MHV-A59. (**A**) Mock-infected (upper panel) and MHV-infected (lower panel) 17 Cl-1 cells were harvested at 2.5, 5 and 8 h p.i.

977 Cytoplasmic lysates were resolved on 10–50% sucrose density gradients. Gradients were
978 fractionated and fractions monitored by absorbance (A_{254} nm). Twelve [numbered] fractions were
979 collected and proteins extracted, resolved by 12% SDS-PAGE and analysed by immunoblotting
980 using the indicated antibodies (anti-S6 as 40S marker, anti-RPL10 as 60S marker, anti-N and anti-
981 S). (**B**) Mock-infected (left panel) and MHV-infected (right panel) 17 Cl-1 cells were harvested at 5
982 h p.i. in high-salt lysis buffer (400 mM KCl) and analysed as described above. Molecular masses
983 (kDa) are indicated on the left. Lane "Inp" contains whole cell lysate.

984 **Figure 6: Effect of GSK-2606414 on MHV-infected cells.** (**A**) 17 Cl-1 mock and MHV-infected
985 cells were treated with 1–5 μM of the GSK-2606414 (PERKi). PERKi was added to the cells
986 immediately after the virus adsorption period was completed and maintained in the medium until
987 cells were harvested 5 h and 8 h later. In the upper panel, cell lysates were separated by 12% SDS-
988 PAGE and immunoblotted using anti-S, anti-p-eIF2α and anti-eIF2α (green fluorescent secondary
989 antibody), and anti-N sera (red fluorescent secondary antibody). In the lower panel, cell lysates
990 were separated by 12% SDS-PAGE and immunoblotted using anti-PERK and anti-N (green
991 fluorescent secondary antibody), and anti-GAPDH sera (red fluorescent secondary antibody).
992 Molecular masses (kDa) are indicated on the left. (**B**) 17 Cl-1 cells infected with MHV-A59 and
993 treated with 0, 2.5 or 5 μM of GSK-2606414 were metabolically pulse-labeled with [^{35}S]Met for 1 h
994 at 5 h p.i. Cells were lysed just after pulse and subjected to 10% SDS-PAGE followed by
995 autoradiography. (**C**) Polysome profiling of MHV-infected cells at 5 h p.i. treated with 5μM of the
996 PERKi. (**D**) Representative images of mock and MHV-infected cells at 5 h p.i. treated with 0, 2.5 or
997 5 μM of GSK-2606414. (**E**) $TCID_{50}$ assays were performed with serial dilutions of the supernatant
998 containing released virions (extracellular) or from extracellular media and cells subjected to a cycle
999 of freezing/thawing (intra- and extracelluar virions) from 17 Cl-1 cells infected with MHV-A59 in
1000 the presence or absence of 5 μM of PERKi. Values show the means of triplicate titrations. Error
1001 bars represent standard errors. All *t*-tests are two-tailed and assume separate variances for the two
1002 populations being compared. (**F**) qRT-PCR of three biological replicates of *BiP* transcripts

normalised by *Rpl19* transcript. Note that the *BiP/Rpl19* transcription ratio is the one plotted (upper panel). RT-PCR analysis of *Xbp-1u* and *Xbp-1s* mRNAs. Total RNA (1µg) was subjected to RT-PCR analysis using primers flanking the *Xbp-1* splice site. PCR products were resolved in a 3% TBE-agarose gel and visualised by ethidium bromide staining. *Rpl19* RT-PCR product was used as a loading control. Molecular size markers (nt) are indicated on the left (lower panel).

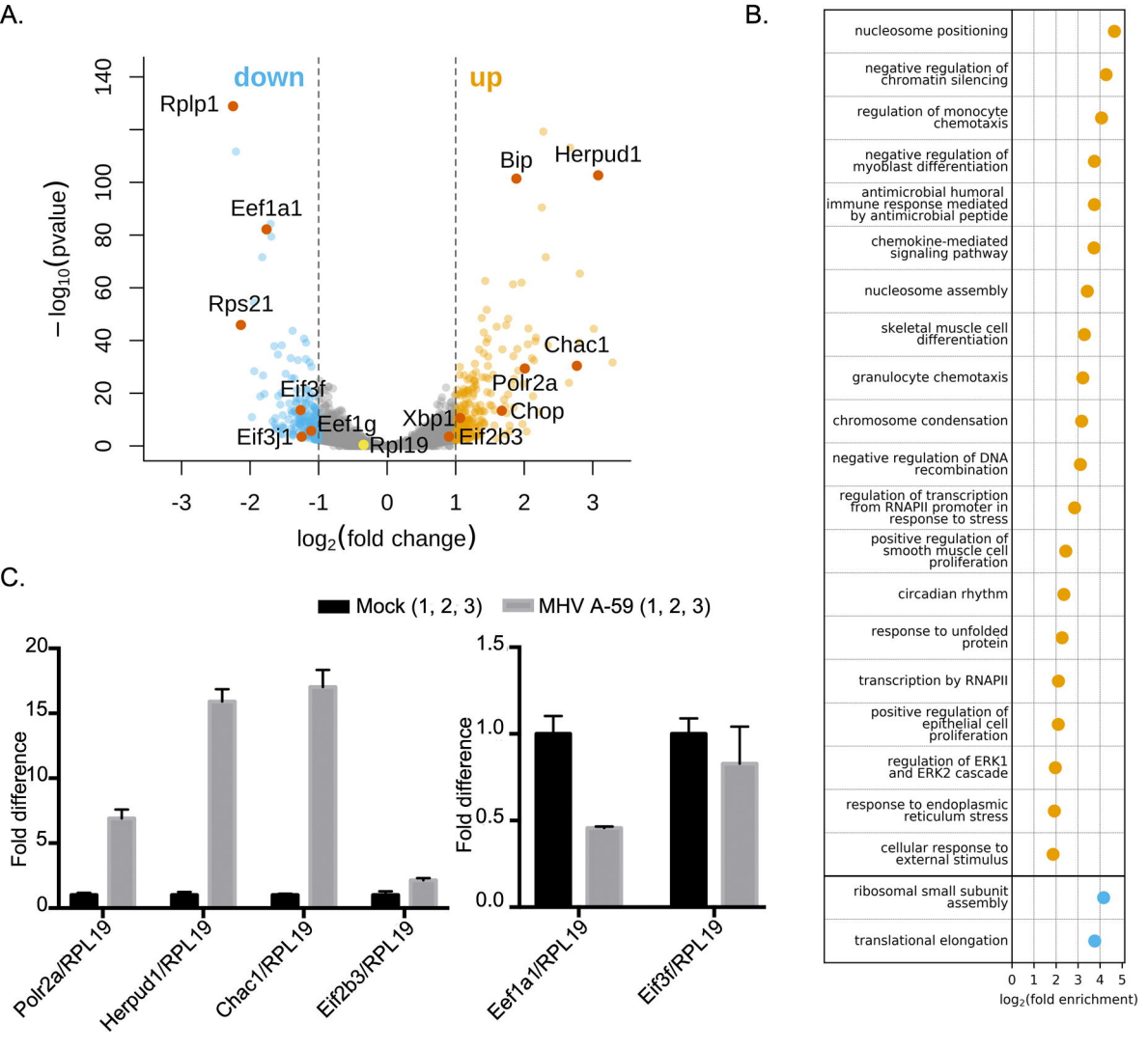
A.
down
up
Rplp1
Eef1a1
Rps21
Eif3f
Eif3j1
Eef1g
Rpl19
Xbp1
Eif2b3
Bip
Herpud1
Chac1
Polr2a
Chop
$-\log_{10}$(pvalue)
$\log_2$(fold change)
B.
nucleosome positioning
negative regulation of chromatin silencing
regulation of monocyte chemotaxis
negative regulation of myoblast differentiation
antimicrobial humoral immune response mediated by antimicrobial peptide
chemokine-mediated signaling pathway
nucleosome assembly
skeletal muscle cell differentiation
granulocyte chemotaxis
chromosome condensation
negative regulation of DNA recombination
regulation of transcription from RNAPII promoter in response to stress
positive regulation of smooth muscle cell proliferation
circadian rhythm
response to unfolded protein
transcription by RNAPII
positive regulation of epithelial cell proliferation
regulation of ERK1 and ERK2 cascade
response to endoplasmic reticulum stress
cellular response to external stimulus
ribosomal small subunit assembly
translational elongation
$\log_2$(fold enrichment)
C.
Mock (1, 2, 3)
MHV A-59 (1, 2, 3)
Fold difference
Polr2a/RPL19
Herpud1/RPL19
Chac1/RPL19
Eif2b3/RPL19
Eef1a1/RPL19
Eif3f/RPL19

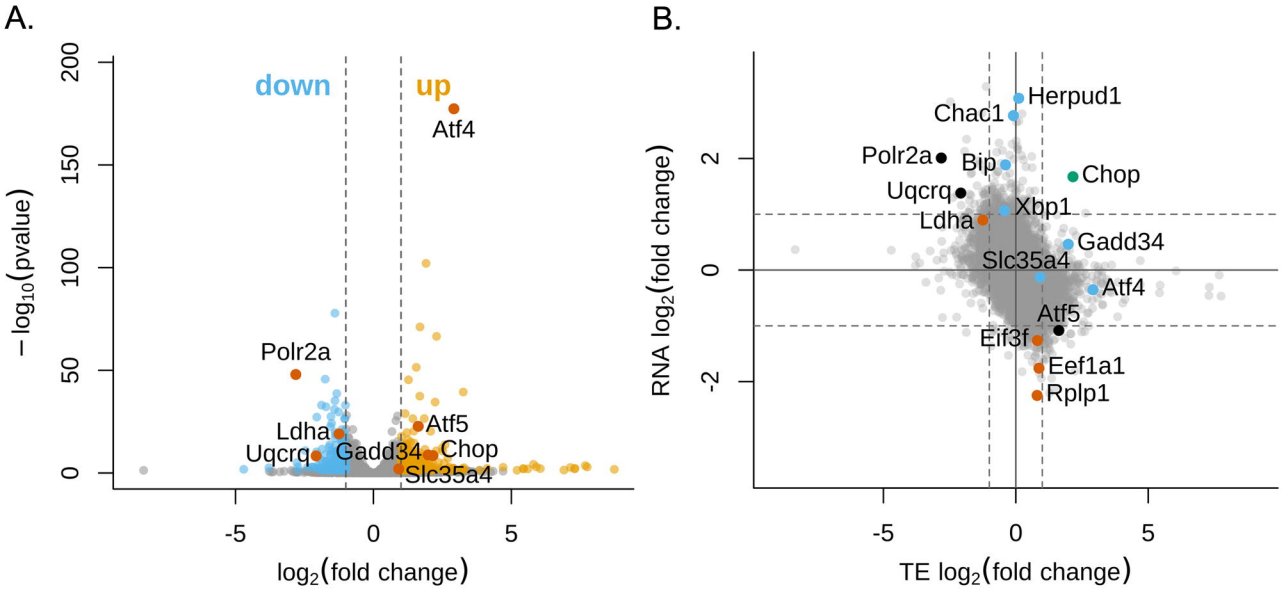
A.
down
up
Atf4
Polr2a
Ldha
Uqcrq
Gadd34
Atf5
Chop
Slc35a4
200
150
100
50
0
− log10(pvalue)
-5
0
5
log2(fold change)
B.
Herpud1
Chac1
Polr2a
Bip
Chop
Uqcrq
Xbp1
Ldha
Gadd34
Slc35a4
Atf4
Atf5
Eif3f
Eef1a1
Rplp1
2
0
-2
RNA log2(fold change)
-5
0
5
TE log2(fold change)

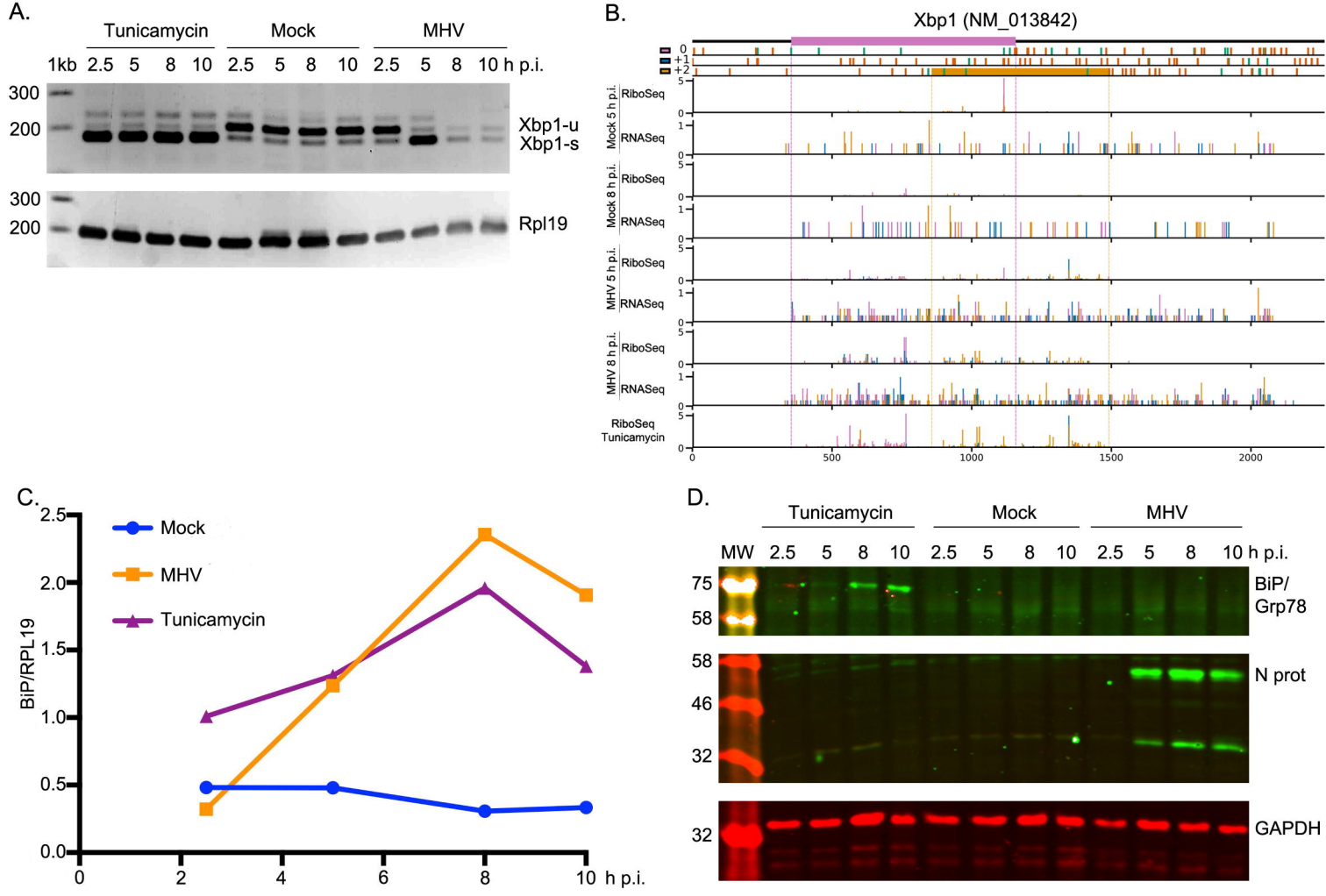
A.
Tunicamycin
Mock
MHV
1kb 2.5 5 8 10 2.5 5 8 10 2.5 5 8 10 h p.i.
300
200
Xbp1-u
Xbp1-s
300
200
Rpl19
B.
Xbp1 (NM_013842)
0
+1
+2
Mock 5 h p.i.
RiboSeq
RNASeq
Mock 8 h p.i.
RiboSeq
RNASeq
MHV 5 h p.i.
RiboSeq
RNASeq
MHV 8 h p.i.
RiboSeq
RNASeq
RiboSeq
Tunicamycin
0
500
1000
1500
2000
C.
Mock
MHV
Tunicamycin
BiP/RPL19
0.0
0.5
1.0
1.5
2.0
2.5
0
2
4
6
8
10 h p.i.
D.
Tunicamycin
Mock
MHV
MW 2.5 5 8 10 2.5 5 8 10 2.5 5 8 10 h p.i.
75
58
BiP/
Grp78
58
46
32
N prot
32
GAPDH

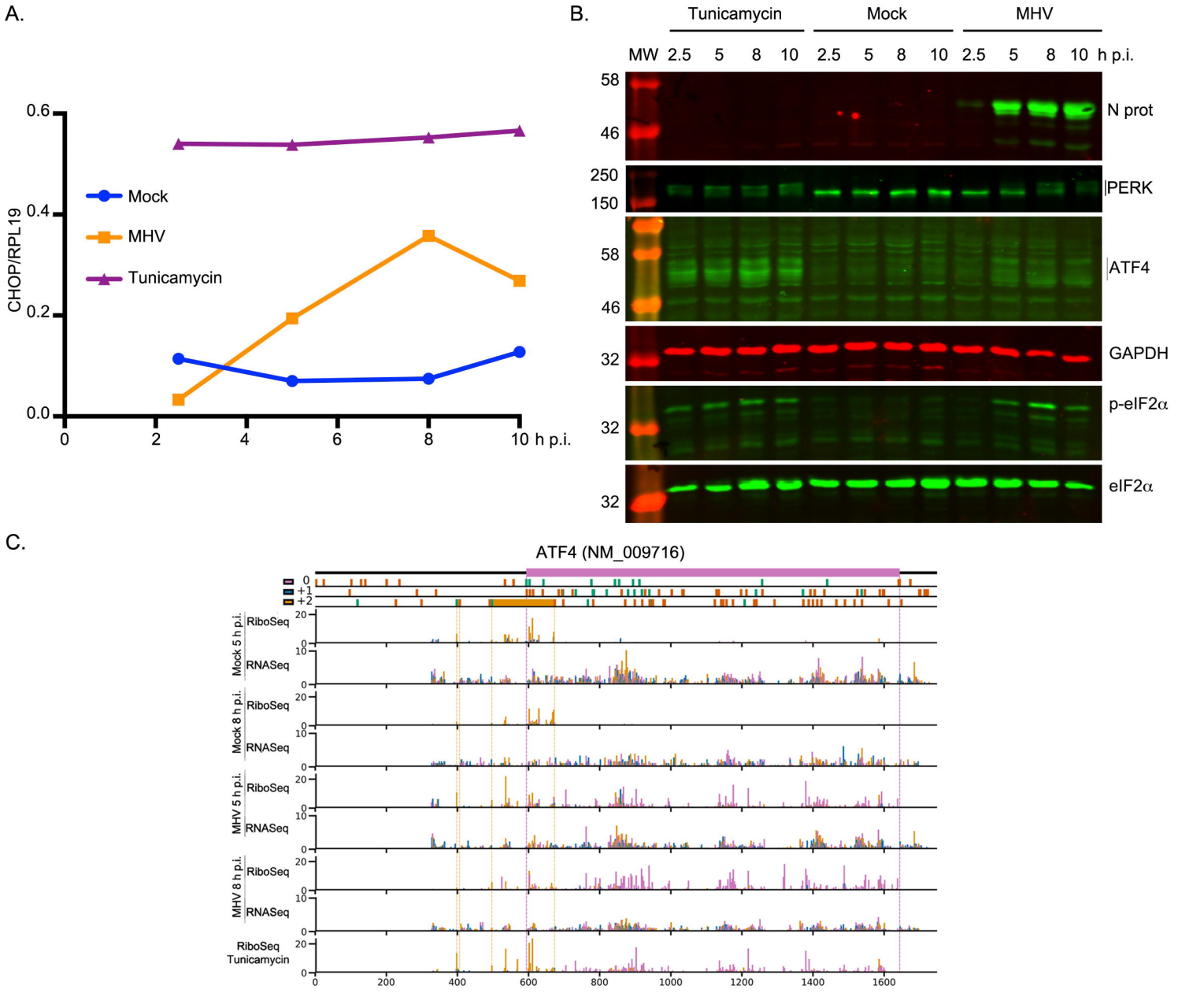
A.
CHOP/RPL19
0.6
0.4
0.2
0.0
Mock
MHV
Tunicamycin
0
2
4
6
8
10 h p.i.
B.
Tunicamycin
Mock
MHV
MW 2.5 5 8 10 2.5 5 8 10 2.5 5 8 10 h p.i.
58
46
250
150
58
46
32
32
32
N prot
PERK
ATF4
GAPDH
p-eIF2α
eIF2α
C.
ATF4 (NM_009716)
0
+1
+2
Mock 5 h p.i.
Mock 8 h p.i.
MHV 5 h p.i.
MHV 8 h p.i.
RiboSeq
RNASeq
RiboSeq Tunicamycin
0
200
400
600
800
1000
1200
1400
1600

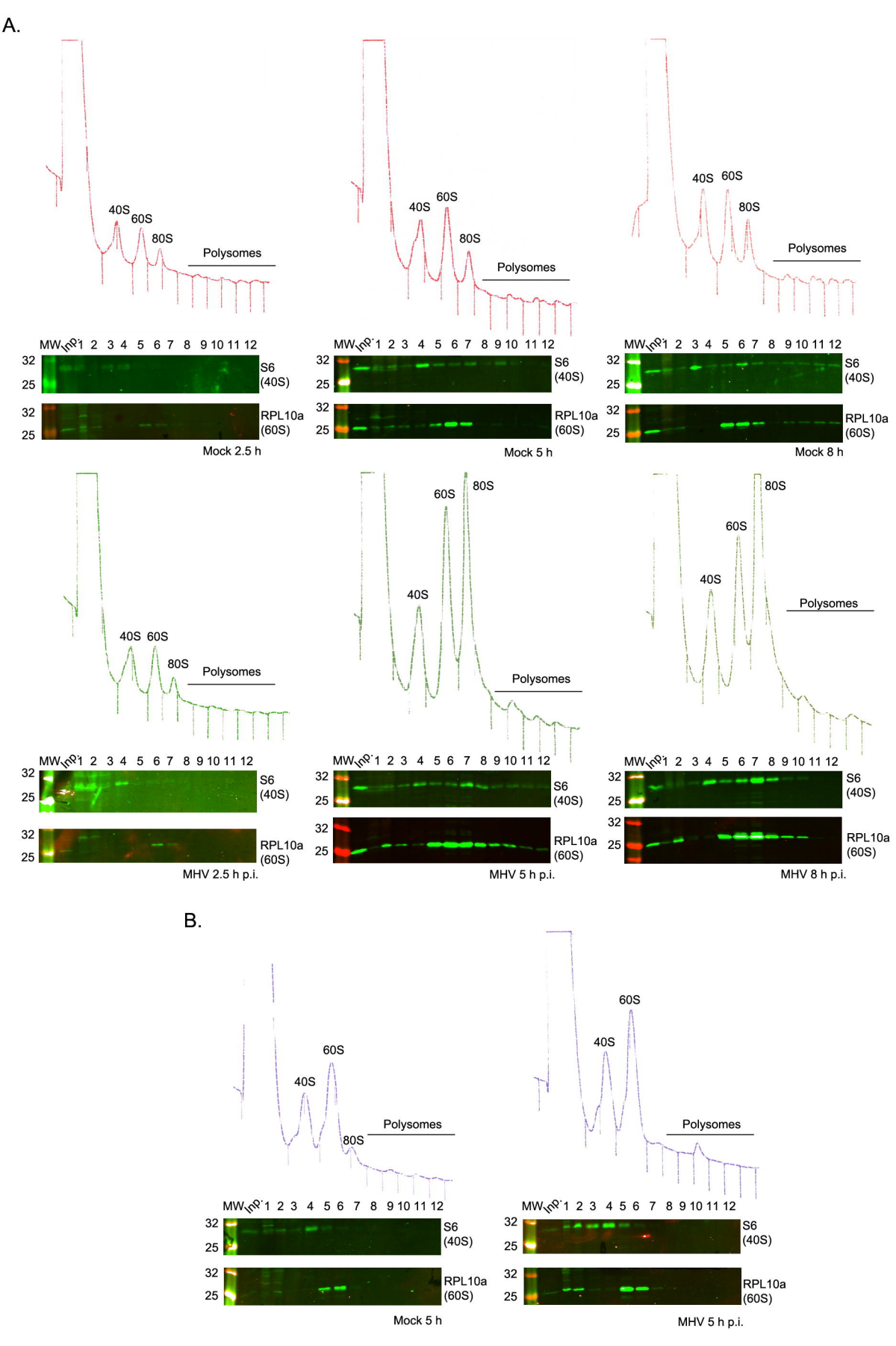
A.
40S
60S
80S
Polysomes
MW
Inp.
1 2 3 4 5 6 7 8 9 10 11 12
32
25
S6
(40S)
RPL10a
(60S)
Mock 2.5 h
Mock 5 h
Mock 8 h
MHV 2.5 h p.i.
MHV 5 h p.i.
MHV 8 h p.i.
B.
Mock 5 h
MHV 5 h p.i.

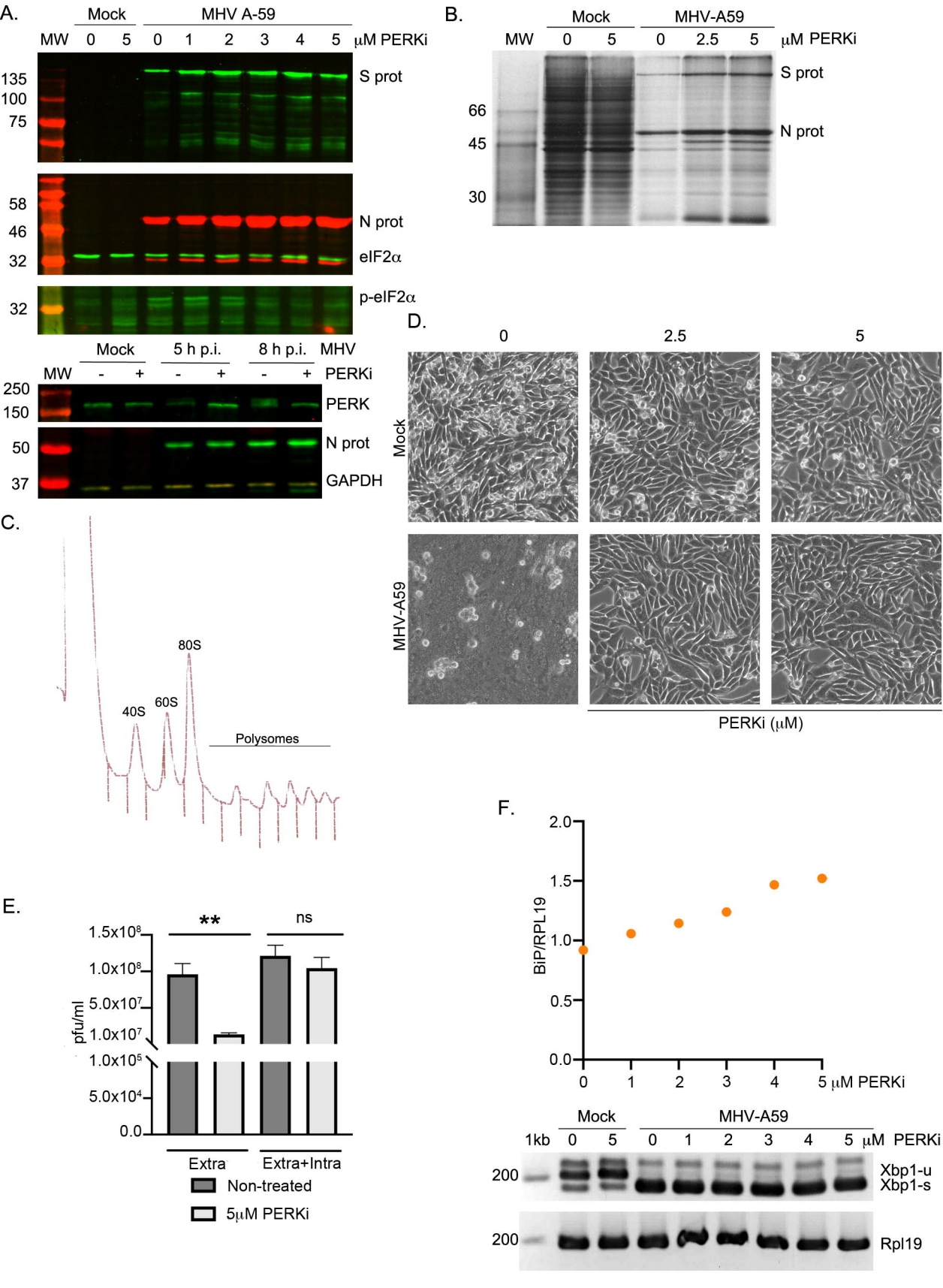
A.
Mock
MHV A-59
MW 0 5 0 1 2 3 4 5 μM PERKi
135
100
75
S prot
58
46
32
N prot
eIF2α
32
p-eIF2α
Mock
5 h p.i.
8 h p.i.
MHV
MW - + - + - + PERKi
250
150
PERK
50
37
N prot
GAPDH
B.
Mock
MHV-A59
MW 0 5 0 2.5 5 μM PERKi
66
45
30
S prot
N prot
C.
80S
60S
40S
Polysomes
D.
0
2.5
5
Mock
MHV-A59
PERKi (μM)
E.
**
ns
1.5x10⁸
1.0x10⁸
5.0x10⁷
1.0x10⁷
1.0x10⁵
5.0x10⁴
0.0
pfu/ml
Extra
Extra+Intra
Non-treated
5μM PERKi
F.
2.0
1.5
1.0
0.5
0.0
BiP/RPL19
0 1 2 3 4 5 μM PERKi
Mock
MHV-A59
1kb 0 5 0 1 2 3 4 5 μM PERKi
200
Xbp1-u
Xbp1-s
200
Rpl19